galaxies

MDPI

Article

Determination of the Hubble Constant and Sound Horizon from Dark Energy Spectroscopic Instrument Year 1 and Dark Energy Survey Year 6 Baryon Acoustic Oscillation

Jose Agustin Lozano Torres [1,2]

[1] Instituto de Física, Universidad Nacional Autónoma de México, Ciudad de México 04510, Mexico; jalozanotorres@gmail.com
[2] Instituto de Astronomía, Universidad Nacional Autónoma de México, Ciudad de México 04510, Mexico

Abstract: We perform new measurements of the expansion rate and the sound horizon at the end of the baryon decoupling, and derive constraints on cosmic key parameters in the framework of the ΛCDM model, wCDM model, non-flat ΛCDM model and the phenomenological emergent dark energy (PEDE) model. We keep r_d and H_0 completely free, and use the recent Dark Energy Spectroscopic Instrument (DESI) Year 1 and Dark Energy Survey (DES) Year 6 BAO measurements in the effective redshift range $0.3 < z < 2.33$, combined with the compressed form of the Pantheon sample of Type Ia supernovae, the latest 34 observational $H(z)$ measurements based on the differential age method, and the recent H_0 measurement from SH0ES 2022 as an additional Gaussian prior. Combining BAO data with the observational $H(z)$ measurements, and the Pantheon SNe Ia data, we obtain $H_0 = 69.70 \pm 1.11$ km s^{-1} Mpc^{-1}, $r_d = 147.14 \pm 2.56$ Mpc in flat ΛCDM model, $H_0 = 70.01 \pm 1.14$ km s^{-1} Mpc^{-1}, $r_d = 146.97 \pm 2.45$ Mpc in PEDE model. The spatial curvature is $\Omega_k = 0.023 \pm 0.025$, and the dark energy equation of state is $w = -1.029 \pm 0.051$, consistent with a cosmological constant. We apply the Akaike information and the Bayesian information criterion test to compare the four models, and see that the PEDE model performs better.

Keywords: Hubble constant; sound horizon; cosmological parameters; numerical methods

Citation: Lozano Torres, J.A. Determination of the Hubble Constant and Sound Horizon from Dark Energy Spectroscopic Instrument Year 1 and Dark Energy Survey Year 6 Baryon Acoustic Oscillation. *Galaxies* **2024**, *12*, 48. https://doi.org/10.3390/galaxies12040048

Received: 31 May 2024
Revised: 6 August 2024
Accepted: 12 August 2024
Published: 13 August 2024

1. Introduction

Observational experiments [1,2] have provided precise estimates of the key parameters of the standard cosmological model ΛCDM. Early measurements [1] estimated the value of the Hubble constant at $H_0 = 67.4 \pm 0.5$ km s^{-1} Mpc^{-1} with an uncertainty of less than 1 km s^{-1} Mpc^{-1}. However, measurements in our local neighborhood of the Hubble constant [3–7] have been improved through the use of cepheid stars in a distance ladder method, leading to a more precise measurement of H_0 as $H_0 = 73.04 \pm 1.04$ km s^{-1} Mpc^{-1} [7]. Despite the success of the ΛCDM model in explaining the current Universe, the measurements of late-time [7] and early-time accelerated cosmic expansion [1] are in tension, with a discrepancy of 4σ–5.7σ. This tension suggests that either the measurements have systematic and calibration issues, or the standard cosmological model needs to be extended with new physics. As a result, various alternative cosmological models have been proposed to address the inconsistencies between cosmological surveys [8–20]. In the opposite directions, many observational studies have been made to provide estimates of the expansion rate, such as quasar lensing [21,22], gravitational-wave events [23–25], fast radio bursts (FRBs) [26,27], Megamaser [28–30], red giant branch tip method (TRGs) [31–33], BAOs [34], etc. [35]. Novel measurements of the Hubble constant independent of the CMB surveys and distance ladder measurements have been performed. A dark siren measurement of the Hubble constant with the LIGO/Virgo gravitational wave event GW190412 and DESI galaxies combined with the bright standard siren measurement from GW170817 estimates $H_0 = 77.96^{+23.0}_{-5.03}$ km s^{-1} Mpc^{-1} [36]. DECam Local Volume Exploration Survey (DELVE)

analyses combined with gravitational wave events from the first three LIGO/Virgo observing runs estimates $H_0 = 68.84^{+15.51}_{-7.74}$ km s^{-1} Mpc^{-1} [37]. Speaking of Baryon Acoustic Oscillations (BAOs), whose measurements from the Dark Energy Spectroscopic Instrument (DESI) and the Dark Energy Survey (DES) play a key role in our analysis, they are sound waves traveling in the primordial plasma, frozen at the recombination epoch. The BAOs surveys gather data on $D_A(z)/r_d$, $D_V(z)/r_d$, $D_M(z)/r_d$, D_H/r_d, and $H(z) \cdot r_d$, with r_d as the comoving sound horizon at the baryon decoupling z_d. The Hubble constant H_0 and the sound horizon r_d are tightly linked, connecting the early- and late-time universe. The sound horizon r_d is determined by early universe conditions and observations from Planck 2018 [1]. An alternative approach to calibrating r_d involves combining BAO data with observations at low redshifts.

In this work, we present the constraints of cosmological key parameters, highlighting measurements of the Hubble constant H_0 and the cosmic sound horizon at the baryon decoupling r_d, where we set the characteristic scale r_d of BAO as a free parameter in the framework of different cosmologies. Without regarding any assumption of the early time physics, we combine the measurement of Baryon Acoustic Oscillations (BAO) in galaxy, quasar, and Lyman-α forest tracers for the first year of observations from the Dark Energy Spectroscopic Instrument (DESI) [38], the BAO measurement for the sixth year of observations from the Dark Energy Survey (DES) [39], the SNe-Ia Pantheon compilation data [40], the observational $H(z)$ data (OHD), and the latest measurement of the Hubble constant performed by SH0ES 2022 as an additional Gaussian prior [7]. The paper is structured as follows: Section 2 presents the cosmological models under study, where will set constraints on cosmic key parameters. Section 3 summarizes our data and methodology. Results on cosmological parameters and constraints are given in Section 4. Finally, we present our discussion and conclusion in Section 5.

2. Theoretical Background

2.1. Flat ΛCDM Model

The Λ cold dark matter (ΛCDM) model takes the dark energy equation-of-state (EoS) as the cosmological constant Λ with $w = -1$, acting as a negative pressure to counteract the effect of gravity. The Friedmann equation for this model is expressed as

$$E^2(z) = \Omega_r(1+z)^4 + \Omega_m(1+z)^3 + \Omega_{DE}(z), \tag{1}$$

where we can set $\Omega_{DE}(z) = \Omega_\Lambda$, with EoS $w = -1$. The Friedmann Equation (1) depends on the free parameters Ω_r, Ω_m, Ω_Λ. The term $E(z)$ is the expansion rate that is the ratio $H(z)/H_0$, where $H(z) = \dot{a}/a$ is the Hubble parameter at redshift z and H_0 is the Hubble constant measured at present time.

2.2. Non-Flat ΛCDM Model

In the ΛCDM model, we depart from the assumption of spatial flatness by introducing a variable curvature parameter Ω_K. In the framework of a Friedmann–Lemaître–Robertson–Walker (FLRW) background, this is analogous to allowing the dark energy density $\Omega_{DE} = 1 - \Omega_m - \Omega_K$ to vary independently from the matter density Ω_m, while maintaining a constant dark-energy EoS with $w = -1$. The Friedmann equation for this model is expressed as

$$E^2(z) = \Omega_r(1+z)^4 + \Omega_m(1+z)^3 + \Omega_K(1+z)^2 + \Omega_{DE}(z). \tag{2}$$

2.3. wCDM Model

The cosmological model wCDM assumes a constant EoS w. The Friedmann equation for wCDM model is expressed as

$$E^2(z) = \Omega_r(1+z)^4 + \Omega_m(1+z)^3 + \Omega_{DE}(1+z)^{3(1+w)}, \tag{3}$$

where Equation (3) depends on the free parameters Ω_r, Ω_m, Ω_Λ, and w. Despite the success of the cosmological constant fitting existing data very well, the small value of Λ relative to the theoretical estimations based on particle physics poses a conflict. This requires going beyond ΛCDM, where dark energy has dynamic-time dependence, hence proposing cosmological models with dark energy EoS parameterized.

2.4. Phenomenological Emergent Dark Energy (PEDE) Model

Generally, the parameterization of a given dark energy EoS w can be a function of redshift z or the scale factor $a(t)$ of the FLRW metric universe, noticing that $1 + z = a_0/a(t)$, where a_0 is the present value of the scale factor. Here, we consider a dynamical dark energy EoS w parameterization called the phenomenological emergent dark energy (PEDE) model. This model introduces a dark energy density, written as

$$\Omega_{DE}(z) = \Omega_{DE} \times [1 - \tanh(\log_{10}(1 + z))], \tag{4}$$

where $\Omega_{DE} = 1 - \Omega_m - \Omega_r$. From the PEDE model, we can write the Friedmann equation in terms of the expansion function as

$$\begin{aligned} E^2(z) = {} & \Omega_r(1+z)^4 + \Omega_m(1+z)^3 \\ & + \Omega_{DE} \times [1 - \tanh(\log_{10}(1 + z))] \end{aligned} \tag{5}$$

where Equation (5) depend on free parameters Ω_r, Ω_m, Ω_{DE}. This dark energy model with zero degrees of freedom as the ΛCDM model acts with no presence in early times, and emerges at later times. We must recall that the PEDE model does not generalize the ΛCDM model. The EoS of this model lies in the phantom region ($w < -1$) in the past and present ($z = 0$), and approximates to the cosmological constant ($w = -1$) in the far future [18].

3. Data and Methodology

In order to estimate and place constraints on the cosmological key parameters in the framework of different cosmologies that we have described above, we use the following observational data sets: the recent BAO measurements performed by DESI year 1, DES year 6, observational $H(z)$ data (OHD), the Pantheon Sample, and the local measurement of the Hubble constant H_0 labeled as R22.

BAO measurements depend on the sound horizon at the epoch of baryon decoupling r_d at $z_d \approx 1060$ in the standard model. It is given by

$$r_d = \frac{1}{H_0} \int_{z_d}^{\infty} \frac{c_s(z)}{E(z)} dz, \tag{6}$$

where the sound speed $c_s(z)$ is a function of the baryon to photon densities ratio, and $E(z)$ is the expansion rate function in terms of our present-day density fraction Ω_r, Ω_m, Ω_{DE}, and Ω_k. The sound horizon r_d is the characteristic scale to calibrate BAO observations, where it is often settled a prior of the CMB measurement. In this analysis, we remove the prior r_d from CMB Planck satellite and set r_d as a free parameter. The BAO measurements from surveys of galaxies, quasars and Lyman-α forest are given by the observables $D_M(z)/r_d$, $D_V(z)/r_d$, and $D_H(z)/r_d$. The transverse comoving distance $D_M(z)$ and the volume angle-average length $D_V(z)$ that quantifies the average of distances measured along are linked to the expansion rate function $E(z)$ by

$$D_M = \frac{c}{H_0} \int_0^z \frac{\mathrm{d}z'}{E(z')}, \tag{7}$$

$$D_V(z) = [z D_H(z) D_M^2(z)]^{1/3}. \tag{8}$$

We use the recent BAO measurements from DESI year 1 data release (DESI DR1) and DES year 6 (DESY6) result, which are performed at a series of redshifts, allowing constrains

on the cosmic key parameters. The DESI DR1 and DESY6 BAO data points are listed in Table 1 with their corresponding redshifts z_{eff}, observables, measurements, and errors.

Table 1. We present the recent 13 BAO measurements from the Dark Energy Spectroscopic Instrument (DESI) year 1 data release and Dark Energy Survey (DES) year 6, on which we perform our analysis.

z_{eff}	Observable	Measurement	Error	Year	Dataset Survey	Reference
0.295	D_V/r_d	7.93	0.15	2024	DESI BGS	[38]
0.510	D_M/r_d	13.62	0.25	2024	DESI LRG	[38]
0.510	D_H/r_d	20.98	0.61	2024	DESI LRG	[38]
0.706	D_M/r_d	16.85	0.32	2024	DESI LRG	[38]
0.706	D_H/r_d	20.08	0.60	2024	DESI LRG	[38]
0.850	D_M/r_d	19.51	0.41	2024	DES Year 6	[39]
0.930	D_M/r_d	21.71	0.28	2024	DESI LRG+ELG	[38]
0.930	D_H/r_d	17.88	0.35	2024	DESI LRG+ELG	[38]
1.317	D_M/r_d	27.79	0.69	2024	DESI ELG	[38]
1.317	D_H/r_d	13.82	0.42	2024	DESI ELG	[38]
1.491	D_V/r_d	26.07	0.67	2024	DESI QSO	[38]
2.330	D_M/r_d	39.71	0.94	2024	DESI Lya QSO	[38]
2.330	D_H/r_d	8.52	0.17	2024	DESI Lya QSO	[38]

In this analysis, we do not take into account the OHD obtained from the measurement of BAO. We only make use of the OHD from differential age method proposed in Ref. [41]. Table 2 shows an updated compilation of OHD covering a total of 34 data points given by the differential age method [41]. We also make use of the Pantheon compilation of 1048 SNe Ia in the redshift range $0.01 < z < 2.3$ [40] and the Hubble constant estimation from the SH0ES team yielding to the Gaussian prior $H_0 = 73.04 \pm 1.04$ km s^{-1} Mpc^{-1} at 68% CL (R22) [7]. To perform our cosmological analysis, we use a nested sampling algorithm tailored for high-dimensional parameter space called Polychord, developed by Handley et al. [42] with the GetDist v1.5.1 [43], as performed in [44,45]. Lastly, we compare our different cosmological models using the Akaike information criterion (AIC) and the Bayesian information Criterion (BIC). The AIC criterion is defined as [46]

$$\mathrm{AIC} = -2\ln(\mathcal{L}_{max}) + 2k + \frac{2k(2k+1)}{N_{tot} - k - 1}, \tag{9}$$

where $\mathcal{L}_{max}$ is the maximum likelihood of the data taken into consideration in which we take the full dataset without the Riess 2022 prior, N_{tot} is the total number of data points, and k is the numbers of parameters. For large N_{tot}, our expression is reduced to

$$\mathrm{AIC} \simeq -2\ln(\mathcal{L}_{max}) + 2k, \tag{10}$$

which is the standard form of the AIC criterion [46]. On the other hand, the Bayesian information criterion is defined as [47]

$$\mathrm{BIC} = -2\ln(\mathcal{L}_{max}) + k\ln N_{tot}. \tag{11}$$

Table 2. We present an update of all 34 $H(z)$ measurements (in units of km s^{-1} Mpc^{-1}) obtained with the differential age method and their associated errors on which we perform our analysis. It is noted that all these measurements are independent, since they come from different datasets.

z	$H(z)$	$\sigma_{H(z)}$	Method	Reference
0.07	69	19.6	Full-spectrum fitting	[48]
0.09	69	12	Full-spectrum fitting	[49]
0.12	68.6	26.2	Full-spectrum fitting	[48]
0.17	83	8	Full-spectrum fitting	[49]

Table 2. *Cont.*

z	$H(z)$	$\sigma_{H(z)}$	Method	Reference
0.179	75	4	Calibrated D4000	[50]
0.199	75	5	Calibrated D4000	[50]
0.20	72.9	29.6	Full-spectrum fitting	[48]
0.27	77	14	Full-spectrum fitting	[49]
0.28	88.8	36.6	Full-spectrum fitting	[48]
0.352	83	14	Calibrated D4000	[50]
0.38	83	13.5	Calibrated D4000	[51]
0.4	95	17	Full-spectrum fitting	[49]
0.4004	77	10.2	Calibrated D4000	[51]
0.4247	87.1	11.2	Calibrated D4000	[51]
0.4497	92.8	12.9	Calibrated D4000	[51]
0.47	89.0	49.6	Full-spectrum fitting	[52]
0.4783	80.9	9	Calibrated D4000	[51]
0.48	97	62	Full-spectrum fitting	[53]
0.5929	104	13	Calibrated D4000	[50]
0.6797	92	8	Calibrated D4000	[50]
0.75	98.8	33.6	Lick indices	[54]
0.7812	105	12	Calibrated D4000	[50]
0.80	113.1	28.5	Full-spectrum fitting	[55]
0.8754	125	17	Calibrated D4000	[50]
0.88	90	40	Full-spectrum fitting	[53]
0.9	117	23	Full-spectrum fitting	[49]
1.037	154	20	Calibrated D4000	[50]
1.26	135	65	Full-spectrum fitting	[56]
1.3	168	17	Full-spectrum fitting	[49]
1.363	160	33.6	Calibrated D4000	[57]
1.43	177	18	Full-spectrum fitting	[49]
1.53	140	14	Full-spectrum fitting	[49]
1.75	202	40	Full-spectrum fitting	[49]
1.965	186.5	50.4	Calibrated D4000	[57]

4. Analysis and Results

To obtain our results, aside from the BAO measurements listed in Table 1 obtained by DESI and DES, we use the Pantheon data given in [40], the latest observational $H(z)$ measurements using the differential age method containing 34 data points listed in Table 2, and the latest Hubble constant measurement, labeled as R22 [7]. We consider the combination of BAO + OHD + Pantheon datasets as the full dataset.

4.1. Flat ΛCDM Model

We present cosmological constraints for the flat ΛCDM model, where $\Omega_k = 0$, $\Omega_\Lambda = 1 - \Omega_m$. We set Ω_m, Ω_Λ, H_0, and r_d as free parameters with the following prior: $\Omega_m \in [0, 1]$, $\Omega_{DE} \in [0, 1 - \Omega_m]$, H_0 (km s^{-1} Mpc^{-1}) $\in [50, 100]$, and r_d (Mpc) $\in [100, 200]$. The recent measurement of the Hubble constant $H_0 = 73.04 \pm 1.04$ km s^{-1} Mpc^{-1} is included into our study as an additional prior, labeled as R22. In Figure 1 our results are depicted at 68% and 95% confidence levels for the posterior distribution in the $\Omega_m - \Omega_\Lambda$, $H_0 - \Omega_m$, and $r_d - H_0$, and contour planes of the standard model of cosmology ΛCDM. In Table 3 are listed our results. Regarding the BAO data alone, the matter density is estimated at 68% C.L. $\Omega_m = 0.262 \pm 0.028$, giving a smaller value than the one estimated by *Planck* 2018 [1], but this has been reported in other studies [38,58,59]. In addition, when we remove DESY6 BAO data point and consider DESI BAO data alone, the matter density is estimated at 68% C.L. $\Omega_m = 0.270 \pm 0.028$. The center panel summarizes the constraints in $\Omega_m - H_0$ plane obtained from the combination of BAO data with R22 prior, and other datasets. All combinations prefer somehow higher values of H_0 and lower ones of matter density Ω_m than the ones estimated by *Planck* [1]. However, they fall in the range of agreement with the values estimated by DESI collaboration [38]. In the right panel, it is noted that combining BAO with OHD and Pantheon or with R22 prior, we break the degeneracy in the $r_d - H_0$ contour plane. The joint analysis of BAO, OHD, and Pantheon, where we refer it as our full dataset, gives the constraint of Hubble constant $H_0 = 69.70 \pm 1.11$ km s^{-1} Mpc^{-1} and

sound horizon at the baryon decoupling $r_d = 147.14 \pm 2.56$ Mpc. By adding Riess 2022 prior for H_0, the fit gives $H_0 = 71.54 \pm 0.71$ km s^{-1} Mpc^{-1} (which is closer to the value measured by SH0ES team 2022 [7]) and $r_d = 144.04 \pm 1.58$ Mpc. Verde et al. [60] finds $r_d = 143.9 \pm 3.1$ Mpc. Lemos et al. Ref. [61] estimates the values of the BAO scale range with the binning method 141.45 Mpc $\leq r_d \leq$ 159.44 Mpc and for the Gaussian method 143.35 Mpc $\leq r_d \leq$ 161.59 Mpc. The various methods used to measure r_d reveal a significant difference between early and late-time observations, similar to the discrepancy seen in H_0 values. An interesting observation is that excluding the Riess 2022 prior leads to H_0 and r_d results that align more closely with those from the *Planck* survey [1].

Table 3. Mean parameters and constraints values at 68% CL for the standard ΛCDM model based on the BAO measurements listed in Table 1, the observational $H(z)$ measurements OHD listed in Table 2, Pantheon SNe Ia data [40], and the Gaussian prior R22 [7].

Parameter	BAO	BAO + OHD + Pantheon	BAO + OHD + Pantheon + R22
H_0 (km s^{-1} Mpc^{-1})	—	69.70 ± 1.11	71.54 ± 0.71
Ω_m	0.263 ± 0.027	0.264 ± 0.016	0.259 ± 0.015
Ω_Λ	0.726 ± 0.020	0.724 ± 0.011	0.728 ± 0.010
r_d (Mpc)	—	147.14 ± 2.56	143.64 ± 1.53

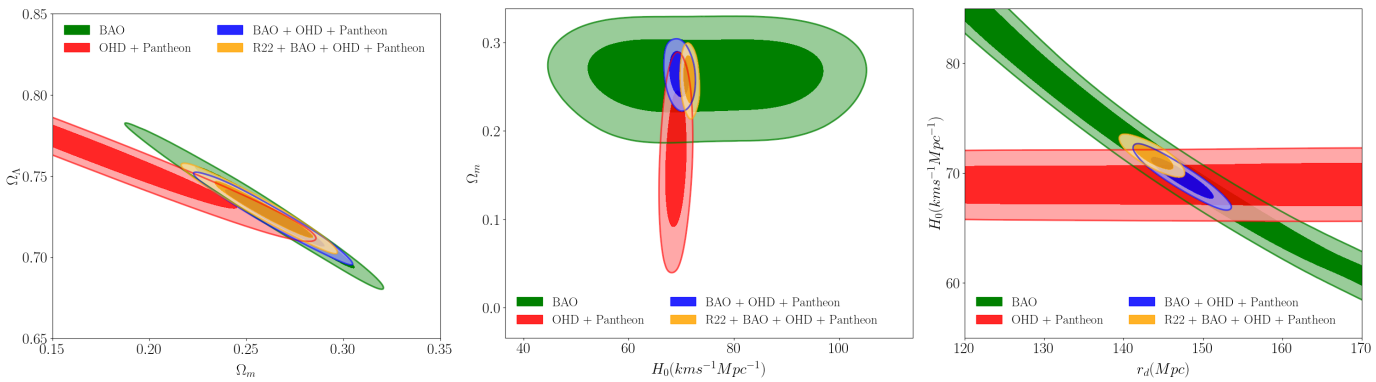

Figure 1. (**Left panel**): Marginalized posterior cosmic constraints on dark energy parameter density Ω_Λ and matter density Ω_m. (**Center panel**): Marginalized posterior cosmic constraints on matter parameter density Ω_m and the Hubble constant H_0, obtained from combining BAO with external data used to calibrate the BAO characteristic scale r_d. (**Right panel**): Marginalized posterior constraints on the sound horizon at the baryon decoupling r_d and the Hubble constant H_0, which shows that R22 prior breaks the degeneracy between r_d and H_0.

4.2. Non-Flat ΛCDM Model

In the non-flat ΛCDM model, we allow the parameter of curvature Ω_k to vary with the prior $\Omega_k \in [-0.1.0.1]$ and $\Omega_m \in [0.1, 1 - \Omega_\Lambda]$. For the other priors, they are the same as for flat ΛCDM model. In Figure 2, we show the 68% and 95% confidence levels for the posterior distribution of the cosmic parameters of our interest and the mean parameter values and 68% C.L. uncertainties derived from the combinations of data sets are listed in Table 4.

In this model, BAO measurements from DESI DR1 and DES Year 6 alone thus measure the parameters (Ω_m, Ω_Λ), finding the following 68% constraints values of $\Omega_m = 0.256 \pm 0.035$, $\Omega_\Lambda = 0.679 \pm 0.032$. Referring to curvature, we find $\Omega_k = 0.055 \pm 0.032$. For the full dataset, we estimate the values of H_0, r_d, and Ω_k at 69.43 ± 1.23 km s^{-1} Mpc^{-1}, 147.65 ± 2.70 Mpc, 0.031 ± 0.028, respectively. The value of Ω_k for all data combinations as listed in Table 4 do not take a negative spatial curvature ($\Omega_k < 0$), which is similar to the DESI result $\Omega_k = 0.065^{+0.068}_{-0.078}$ [38] and different from the results obtained by *Planck* for CMB alone [1]. The estimated results are very close to zero, so they do not rule out a flat universe.

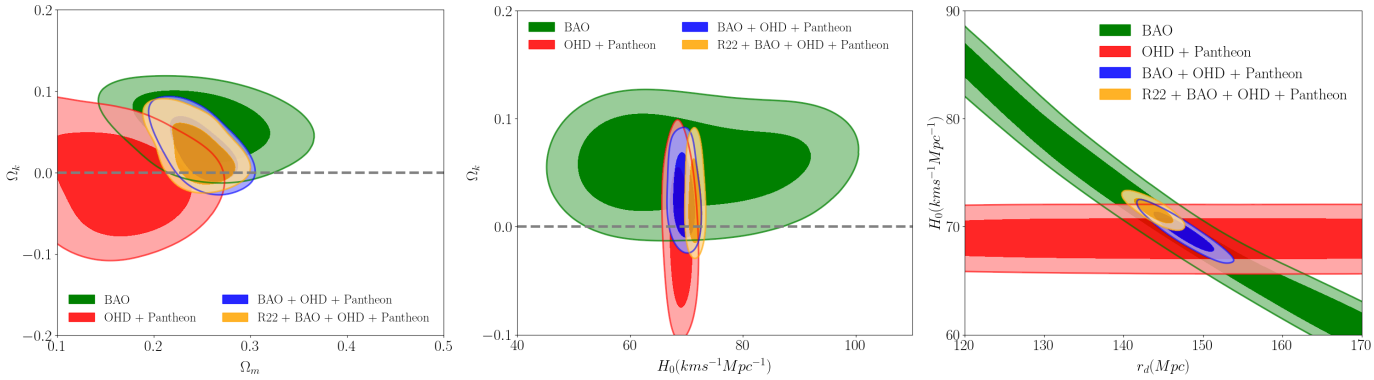

Figure 2. Constraints on different cosmic parameters in the non-flat ΛCDM model. (**Left panel**): 68% and 95% marginalized posterior cosmic constraints on Ω_k-Ω_m plane. (**Center panel**): 68% and 95% marginalized posterior cosmic constraints on Ω_k-H_0 plane. (**Right panel**): 68% and 95% marginalized posterior constraints on the sound horizon at the baryon decoupling r_d and the Hubble constant H_0, which shows that R22 prior breaks the degeneracy between r_d and H_0.

Table 4. Mean parameters and constraints values at 68% CL for the ΛCDM model with free spatial curvature based on the BAO measurements listed in Table 1, the observational $H(z)$ measurements OHD listed in Table 2, Pantheon SNe Ia data [40], and the Gaussian prior R22 [7].

Parameter	BAO	BAO + OHD + Pantheon	BAO + OHD + Pantheon + R22
H_0 (km s^{-1} Mpc^{-1})	—	69.43 ± 1.23	71.48 ± 0.76
Ω_m	0.256 ± 0.035	0.249 ± 0.022	0.246 ± 0.020
Ω_Λ	0.679 ± 0.032	0.706 ± 0.020	0.716 ± 0.019
Ω_k	0.055 ± 0.032	0.031 ± 0.028	0.023 ± 0.025
r_d (Mpc)	—	147.65 ± 2.70	143.76 ± 1.56

4.3. wCDM Model

In Figure 3, we show the 68% and 95% confidence levels for the posterior distribution of the cosmic parameters of our interest and the mean parameter values and 68% C.L. uncertainties derived from the combinations of data sets are listed in Table 5.

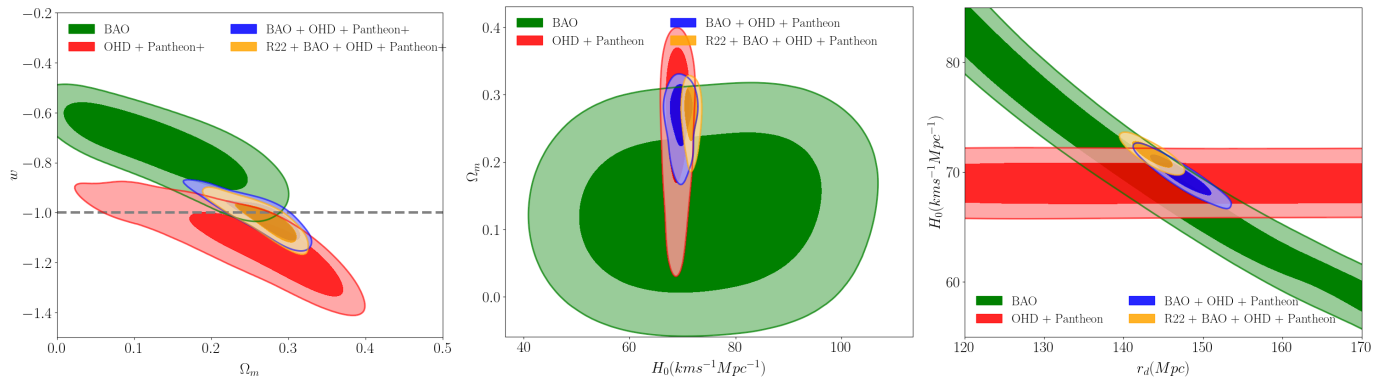

Figure 3. (**Left panel**): 68% and 95% marginalized posterior cosmic constraints on Ω_m-w plane. (**Center panel**): 68% and 95% marginalized posterior cosmic constraints on Ω_m-H_0 plane. (**Right panel**): 68% and 95% marginalized posterior constraints on the sound horizon at the baryon decoupling r_d and the Hubble constant H_0, which shows that R22 prior breaks the degeneracy between r_d and H_0.

Table 5. Constraints at 68% CL on the cosmological parameters for the wCDM model based on the BAO measurements listed in Table 1, the observational $H(z)$ measurements OHD listed in Table 2, Pantheon SNe Ia data, and the Gaussian prior R22.

Parameter	BAO	BAO + OHD + Pantheon	BAO + OHD + Pantheon + R22
H_0 (km s^{-1} Mpc^{-1})	—	69.65 ± 1.20	71.50 ± 0.80
Ω_m	0.125 ± 0.094	0.273 ± 0.027	0.269 ± 0.026
Ω_Λ	0.830 ± 0.072	0.717 ± 0.020	0.720 ± 0.019
w	-0.725 ± 0.119	-1.026 ± 0.054	-1.029 ± 0.051
r_d (Mpc)	—	147.24 ± 2.36	143.83 ± 1.78

In the left panel of Figure 3 we show the constraints on Ω_m and w derived from the latest DESI and DES BAO measurements and combinations, while the center and right panel show the corresponding bounds on r_d and H_0. In the plane $\Omega_m - w$, we find for the full dataset $\Omega_m = 0.273 \pm 0.027$, $w = -1.026 \pm 0.054$, while combining the full dataset with the R22 prior for H_0, the constraint on w leads to $w = -1.029 \pm 0.051$. Therefore, we observe that the dark energy equation of state we obtain for the full dataset is in agreement with the value estimated by the CMB Planck satellite [1], which results in $w = -1.030 \pm 0.03$, consistent with a cosmological constant. However, when we consider BAO alone and BAO + R22, the equation of state is 2σ away from the cosmological constant, which result in $w = -0.744 \pm 0.120$, $w = -0.725 \pm 0.119$, respectively. Although these results are obtained in the wCDM model, they are consistent with the results from DESI collaboration [38] when the equation of state is allowed to vary with time $w(a) = w_0 + (1 - a)w_a$ where DESI data prefer solutions $w_0 > -1$ and $w_a < 0$, but this will require further investigation. Referring to the center and right panel in Figure 3, we observe that the sound horizon at the baryon decoupling r_d and the Hubble constant H_0 regarding the full dataset tend to be in agreement with the values estimated by *Planck* [1], while combining the full dataset with R22 prior for H_0, we find $r_d = 143.83 \pm 1.78$ Mpc, which is consistent with other results performed by Pogosian et al., Nunes et al., and Verde et al. [58,60,62].

4.4. Phenomenological Emergent Dark Energy Model

Motivated by the current issues of cosmological observations of the accelerated cosmic expansion, a new model which proposes dark energy with no effective presence in the past and emerging at later times has caught the attention [18]. This dark energy model with zero degrees of freedom (similar to the ΛCDM) is called phenomenological emergent dark energy. We show our results in Figure 4, in which we show the 68% and 95% confidence levels for the posterior distribution of the cosmic parameters of our interest and the mean parameter values and 68% C.L. uncertainties derived from the combinations of data sets are listed in Table 6.

Table 6. Mean parameters and constraints values at 68% CL for the Phenomenological Emergent Dark Energy (PEDE) model based on the BAO measurements listed in Table 1, the observational $H(z)$ measurements OHD listed in Table 2, Pantheon SNe Ia data, and the Gaussian prior R22.

Parameter	BAO	BAO + OHD + Pantheon	BAO + OHD + Pantheon + R22
H_0 (km s^{-1} Mpc^{-1})	—	70.01 ± 1.14	71.79 ± 0.79
Ω_m	0.283 ± 0.017	0.315 ± 0.007	0.312 ± 0.008
Ω_Λ	0.713 ± 0.014	0.682 ± 0.007	0.685 ± 0.006
r_d (Mpc)	—	146.97 ± 2.45	144.55 ± 1.56

In BAO data alone, the matter density parameter results in $\Omega_m = 0.283 \pm 0.017$, which is consistent with the value obtained by DESI ($\Omega_m = 0.295 \pm 0.015$) [38]. However, the full dataset gives the value of $\Omega_m = 0.315 \pm 0.007$ and $\Omega_\Lambda = 0.682 \pm 0.007$, which are in excellent agreement with those obtained by *Planck* [1]. Additionally, the Hubble constant is found to be higher at $H_0 = 70.01 \pm 1.14$ km s^{-1} Mpc^{-1}, which falls between the *Planck* and

SH0ES 2022 measurements of the Hubble constant and is found to be in agreement with measurements from the tip of the red giant branch performed by Freeman et al. [31–33]. By incorporating the R22 prior for H_0, the fit gives a result in accord with the value obtained by SH0ES 2022 [7], while the sound horizon r_d is lower in comparison with *Planck*: $H_0 = 71.69 \pm 0.71$ km s^{-1} Mpc^{-1} and $r_d = 144.55 \pm 1.56$ Mpc. Additionally, the matter and dark energy densities also are in agreement with the values reported by *Planck* [1], and we do not see a tension in these parameters as it was reported by Shafieloo et al. [18].

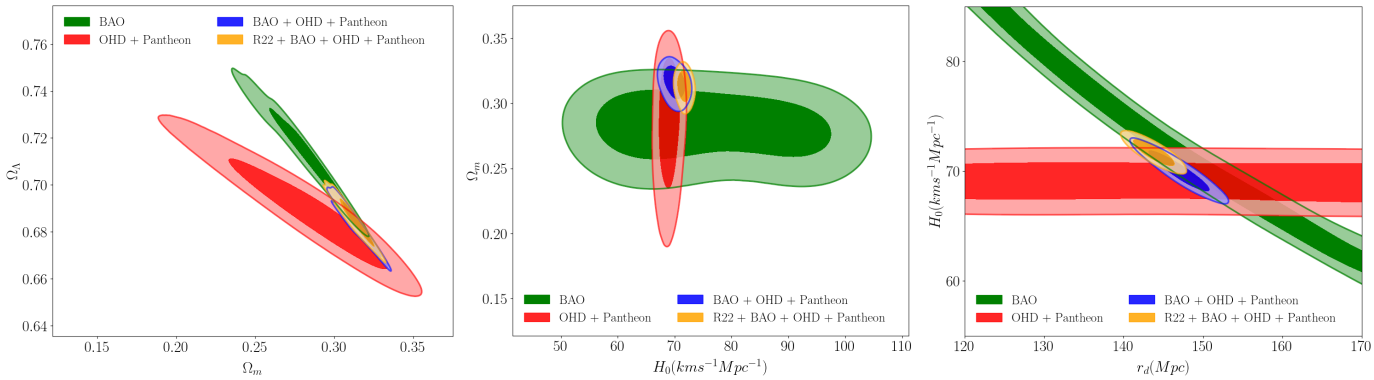

Figure 4. Constraints on different cosmic parameters in the PEDE model. (**Left panel**): 68% and 95% marginalized posterior cosmic constraints on Ω_Λ-Ω_m plane. (**Center panel**): 68% and 95% marginalized posterior cosmic constraints on Ω_m-H_0 plane. (**Right panel**): 68% and 95% marginalized posterior constraints on the sound horizon at the baryon decoupling r_d and the Hubble constant H_0, which shows that R22 prior breaks the degeneracy between r_d and H_0.

5. Discussion

In this work, we have provided new measurements on the Hubble constant and sound horizon using the recent BAO measurements from different tracers of the matter density in seven redshift bins performed by the Dark Energy Spectroscopic Instrument DESI year 1 data release [38], the angular diameter distance measurement obtained with the Baryonic Acoustic Oscillation feature from galaxy clustering in the completed Dark Energy Survey, consisting of six years (Y6) of observations [39], the observational $H(z)$ data, the Pantheon SNe Ia sample, and the R22 prior.

For the full dataset, we determine the Hubble constant and sound horizon values to be $H_0 = 69.70 \pm 1.11$ km s^{-1} Mpc^{-1}, $r_d = 147.14 \pm 2.56$ Mpc^{-1} in the standard flat ΛCDM model, $H_0 = 69.43 \pm 1.23$ km s^{-1} Mpc^{-1}, $r_d = 147.65 \pm 2.70$ Mpc^{-1} in the non-flat ΛCDM, and $H_0 = 69.65 \pm 1.20$ km s^{-1} Mpc^{-1}, $r_d = 147.24 \pm 2.36$ Mpc^{-1} in the flat wCDM model. The most interesting results are in the phenomenological emergent dark energy PEDE model: combining the full dataset with the R22 prior for H_0, the matter density parameter is $\Omega_m = 0.315 \pm 0.007$, the dark energy density parameter $\Omega_\Lambda = 0.682 \pm 0.007$, the Hubble constant $H_0 = 71.79 \pm 0.79$ km s^{-1} Mpc^{-1}, and the sound horizon $r_d = 144.55 \pm 1.56$, alleviating the tension from those measured in combination with the CMB full dataset [18]. This is important, as this PEDE model results from our data align with cosmological observations at low [38] and high redshifts [1], which can be a good alternative to explain the effective behavior of dark energy in comparison with the cosmological constant Λ. The DESI collaboration has recently presented findings suggesting a potential deviation from the standard model of cosmology, ΛCDM, at the 3.9σ level [38]. Utilizing the first-year data release from DESI, combined with additional cosmological datasets, several recent studies have explored the characteristics of dark energy and applied constraints to its behavior [63–68]. These investigations have involved the use of parameterized models, such as the Chevallier–Polarski–Linder (CPL) model, quintessence, Chaplying gas model, and Taylor-expanded dark models, among others. However, the adequacy of the recent DESI year 1 data release in rejecting the standard

cosmological model remains uncertain. Consequently, forthcoming DESI data releases will be essential for comprehensively characterizing the evolution of dark energy.

Comparing our models, we calculate the AIC and BIC for the PEDE, flat ΛCDM, non-flat ΛCDM, and wCDM models. The results are listed in Table 7. Table 7 shows that the lowest values of AIC and BIC correspond to the PEDE model, as well as ΔAIC and ΔBIC having negative values. Therefore, the PEDE model performs better than the reference model flat ΛCDM model and the rest of the models. Consequently, making the comparison of our results with other studies, we see that our values are consistent with DESI collaboration official results [38] for the same models studied there by the inclusion of the observation $H(z)$ measurements (OHD) and R22 prior and the exclusion of the CMB full dataset. As for the PEDE model, the tension remaining in the estimation of the matter density reported in [18] vanishes by incorporating the BAO measurements performed by DESI and DES disregarding the CMB full dataset. In conclusion, the BAO information obtained by DESI and DES demonstrates an enormous power for deriving values and constraints of the cosmological parameters when combined with other estimations for the sound horizon and Hubble constant.

Table 7. The table presents the values of Akaike information criterion (AIC), the Bayesian information criterion (BIC), and the differences of ΔAIC and ΔBIC for each model by taking flat ΛCDM model as our reference model.

Model	AIC	BIC	ΔAIC	ΔBIC
Flat ΛCDM	92.536	93.276	0	0
Non-flat ΛCDM	94.977	96.027	2.441	2.751
wCDM	94.468	95.518	1.932	2.242
PEDE	91.657	92.398	−0.879	−0.878

Funding: This research received no external funding.

Institutional Review Board Statement: Not applicable.

Informed Consent Statement: Not applicable.

Data Availability Statement: The data underlying this article is already given with references during the analysis of this work.

Acknowledgments: We would like to thank CONAHCYT for sponsoring this project.

Conflicts of Interest: The author declares no conflicts of interest. The funders had no role in the design of the study; in the collection, analyses, or interpretation of data; in the writing of the manuscript; or in the decision to publish the results.

References

1. Planck Collaboration. Planck 2018 Results—VI. Cosmological Parameters. *Astron. Astrophys.* **2020**, *A6*, 641.
2. Bennett, C.L.; Larson, D.; Weil, J.L.; Jarosik, N.; Hinshaw, G.; Odegard, N.; Smith, K.M.; Hill, R.S.; Gold, B.; Halpern, M.; et al. Nine-year Wilkinson microwave anisotropy probe (WMAP) observations: Final maps and results. *Astrophys. J. Suppl. Ser.* **2013**, *208*, 20. [CrossRef]
3. Riess, A.G.; Filippenko, A.V.; Challis, P.; Clocchiatti, A.; Diercks, A.; Garnavich, P.M.; Gillil, R.L.; Hogan, C.J.; Jha, S.; Kirshner, R.P.; et al. Observational Evidence from Supernovae for an Accelerating Universe and a Cosmological Constant. *Astron. J.* **1998**, *116*, 1009. [CrossRef]
4. Riess, A.G.; Macri, L.; Casertano, S.; Lampeitl, H.; Ferguson, H.C.; Filippenko, A.V.; Jha, S.W.; Li, W.; Chornock, R. A 3% solution: Determination of the Hubble constant with the Hubble space telescope and wide field camera 3. *Astron. J.* **2011**, *730*, 119. [CrossRef]
5. Riess, A.G.; Macri, L.M.; Hoffmann, S.L.; Scolnic, D.; Casertano, S.; Filippenko, A.V.; Tucker, B.E.; Reid, M.J.; Jones, D.O.; Silverman, J.M.; et al. A 2.4% determination of the local value of the Hubble constant. *Astron. J.* **2016**, *826*, 56. [CrossRef]
6. Riess, A.G.; Casertano, S.; Yuan, W.; Macri, L.M.; Scolnic, D. Large Magellanic Cloud Cepheid Standards Provide a 1% Foundation for the Determination of the Hubble Constant and Stronger Evidence for Physics beyond ΛCDM. *Astron. J.* **2019**, *876*, 55. [CrossRef]

7. Riess, A.G.; Yuan, W.; Macri, L.M.; Scolnic, D.; Brout, D.; Casertano, S.; Jones, D.O.; Murakami, Y.; Anand, G.S.; Breuval, L.; et al. A Comprehensive Measurement of the Local Value of the Hubble Constant with 1 km/s/Mpc Uncertainty from the Hubble Space Telescope and the SH0ES Team. *Astrophys. J. Lett.* **2022**, *934*, L7. [CrossRef]
8. Huang, Q.G.; Wang, K. How the dark energy can reconcile Planck with local determination of the Hubble constant. *Eur. Phys. J.* **2016**, *76*, 506. [CrossRef]
9. Di Valentino, E.; Melchiorri, A.; Silk, J. Reconciling Planck with the local value of H0 in extended parameter space. *Phys. Lett. B* **2016**, *761*, 242–246. [CrossRef]
10. Xu, L.; Huang, Q.G. Detecting the neutrinos mass hierarchy from cosmological data. *Sci. China Phys. Mech. Astron.* **2018**, *61*, 039521. [CrossRef]
11. Yang, W.; Pan, S.; Di Valentino, E.; Saridakis, E.N.; Chakraborty, S. Observational constraints on one-parameter dynamical dark-energy parametrizations and the H_0 tension. *Phys. Rev. D* **2019**, *99*, 043543. [CrossRef]
12. Poulin, V.; Smith, T.L.; Karwal, T.; Kamionkowsk, M. Early Dark Energy can Resolve the Hubble Tension. *Phys. Rev. Lett.* **2019**, *122*, 221301. [CrossRef] [PubMed]
13. Vagnozzi, S. New physics in light of the H_0 tension: An alternative view. *Phys. Rev. D* **2020**, *102*, 023518. [CrossRef]
14. Liu, M.; Huang, Z.; Luo, X.; Miao, H.; Singh, N.K.; Huang, L. Can non-standard recombination resolve the Hubble tension? *Sci. China Phys. Mech. Astron.* **2020**, *63*, 290405. [CrossRef]
15. Ding, Q.; Nakama, T.; Wang, Y. A gigaparsec-scale local void and the Hubble tension. *Sci. China Phys. Mech. Astron.* **2020**, *63*, 290403. [CrossRef]
16. Ryan, J.; Chen, Y.; Ratra, B. Baryon acoustic oscillation, Hubble parameter, and angular size measurement constraints on the Hubble constant, dark energy dynamics, and spatial curvature. *Mon. Not. R. Astron. Soc.* **2019**, *488*, 3844–3856. [CrossRef]
17. Zhao, G.B.; Raveri, M.; Pogosian, L.; Wang, Y.; Crittenden, R.G.; Handley, W.J.; Percival, W.J.; Beutler, F.; Brinkmann, J.; Chuang, C.; et al. Dynamical dark energy in light of the latest observations. *Nat. Astron.* **2017**, *1*, 627–632. [CrossRef]
18. Li, X.; Shafieloo, A. A Simple Phenomenological Emergent Dark Energy Model can Resolve the Hubble Tension. *Astrophys. J. Lett.* **2019**, *883*, L3. [CrossRef]
19. Di Valentino, E. Investigating Cosmic Discordance. *Astrophys. J. Lett.* **2021**, *908*, L9. [CrossRef]
20. Haitao, M.; Zhiqi, H. The H_0 Tension in Non-flat QCDM Cosmology. *Astron. J.* **2018**, *868*, 20.
21. Millon, M.; Galan, A.; Courbin, F.; Treu, T.; Suyu, S.H.; Ding, X.; Birrer, S.; Chen, G.C.-F.; Shajib, A.J.; Sluse, D.; et al. An exploration of systematic uncertainties in the inference of H_0 from time-delay cosmography. *Astron. Astrophys.* **2020**, *639*, A101. [CrossRef]
22. Wong, K.C.; Suyu, S.H.; Chen, G.C.-F.; Rusu, C.E.; Millon, M.; Sluse, D.; Bonvin, V.; Fassnacht, C.D.; Taubenberger, S.; Auger, M.W.; et al. H0LiCOW—XIII. A 2.4 percent measurement of H_0 from lensed quasars: 5.3σ tension between early- and late-Universe probes. *Mon. Not. R. Astron. Soc.* **2020**, *498*, 1420–1439. [CrossRef]
23. Mooley, K.P.; Deller, A.T.; Gottlieb, O.; Nakar, E.; Hallinan, G.; Bourke, S.; Frail, D.A.; Horesh, A.; Corsi, A.; Hotokezaka, K. Superluminal motion of a relativistic jet in the neutron-star merger GW170817. *Nature* **2018**, *561*, 355–359. [CrossRef] [PubMed]
24. The LIGO Scientific Collaboration and The Virgo Collaboration; The 1M2H Collaboration; The Dark Energy Camera GW-EM Collaboration and the DES Collaboration; The DLT40 Collaboration; The Las Cumbres Observatory Collaboration; The VINROUGE Collaboration; The MASTER Collaboration. A gravitational-wave standard siren measurement of the Hubble constant. *Nature* **2017**, *551*, 85–88. [CrossRef] [PubMed]
25. Hotokezaka, K.; Nakar, E.; Gottlieb, O.; Nissanke, S.; Masuda, K.; Hallinan, G.; Mooley, K.P.; Deller, A.T. A Hubble constant measurement from the superluminal motion of the jet in GW170817. *Nat. Astron.* **2019**, *3*, 940–944. [CrossRef]
26. Wu, Q.; Zhang, G.-Q.; Wang, F.-Y. An 8 percent determination of the Hubble constant from localized fast radio bursts. *Mon. Not. R. Astron. Soc. Lett.* **2022**, *515*, L1–L5. [CrossRef]
27. James, C.W.; Ghosh, E.M.; Prochaska, J.X.; Bannister, K.W.; Bhari, S.; Day, C.K.; Deller, A.T.; Glowacki, M.; Gordon, A.C.; Heintz, K.E.; et al. A measurement of Hubble's Constant using Fast Radio Bursts. *Mon. Not. R. Astron. Soc.* **2022**, *516*, 4862–4881. [CrossRef]
28. Pesce, D.W.; Braatz, J.A.; Reid, M.J.; Riess, A.G.; Scolnic, D.; Condon, J.J.; Gao, F.; Henkel, C.; Impellizzeri, C.M.V.; Kuo, C.Y.; et al. The Megamaser Cosmology Project. XIII. Combined Hubble Constant Constraints. *Astrophys. J. Lett.* **2020**, *891*, L1. [CrossRef]
29. Reid, J.; Pesce, D.W.; Riess, A.G. An Improved Distance to NGC 4258 and Its Implications for the Hubble Constant. *Astrophys. J. Lett.* **2019**, *886*, L27. [CrossRef]
30. Kuo, C.Y.; Braatz, J.A.; Lo, K.Y.; Reid, M.J.; Suyu, S.H.; Pesce, D.W.; Condon, J.J.; Henkel, C.; Impellizzeri, C.M.V. The Megamaser Cosmology Project. VI. Observations of NGC 6323. *Astron. J.* **2015**, *800*, 26. [CrossRef]
31. Freedman, W.L.; Madore, B.F.; Hatt, D.; Hoyt, T.J.; Jang, I.S.; Beaton, R.L.; Burns, C.R.; Lee, M.G.; Monson, A.J.; Neeley, J.R.; et al. The Carnegie-Chicago Hubble Program. VIII. An Independent Determination of the Hubble Constant Based on the Tip of the Red Giant Branch. *Astron. J.* **2019**, *882*, 34. [CrossRef]
32. Freedman, W.L.; Madore, B.F.; Hoyt, T.; Jang, I.S.; Beaton, R.; Lee, M.G.; Monson, A.; Neeley, J.; Jeffrey, R. Calibration of the Tip of the Red Giant Branch. *Astron. J.* **2020**, *891*, 57. [CrossRef]
33. Freedman, W.L. Measurements of the Hubble Constant: Tensions in Perspective. *Astron. J.* **2021**, *919*, 16. [CrossRef]
34. Addison, G.E.; Watts, D.J.; Bennett, C.L.; Halpern, M.; Hinshaw, G.; Weil, J.L. Elucidating ΛCDM: Impact of Baryon Acoustic Oscillation Measurements on the Hubble Constant Discrepancy. *Astron. J.* **2021**, *853*, 119. [CrossRef]

35. Moresco, M.; Amati, L.; Amendola, L.; Birrer, S.; Blakeslee, J.P.; Cantiello, M.; Cimatti, A.; Darling, J.; Valle, M.D.; Fishbach, M.; et al. Unveiling the Universe with emerging cosmological probes. *Living Rev. Relativ.* **2022**, *25*, 6.
36. Ballard, W.; Palmese, A.; Magaña, I.; BenZvi, S.; Moon, J.; Ross, A.J.; Rossi, G.; Aguilar, J.; Ahlen, S.; Blum, R.; et al. A dark siren measurement of the Hubble constant with the LIGO/Virgo gravitational wave event GW190412 and DESI galaxies. *arXiv* **2023**, arXiv:2311.13062.
37. Alfradique, V.; Bom, C.R.; Palmese, A.; Teixeira, G.; Santana-Silva, L.; Drlica-Wagner, A.; Riley, A.H.; Rossi, G.; Martínez-Vázquez, C.E.; Sand, D.J.; et al. A dark siren measurement of the Hubble constant using gravitational wave events from the first three LIGO/Virgo observing runs and DELVE. *Mon. Not. R. Astron. Soc.* **2024**, *528*, 3249–3259. [CrossRef]
38. DESI Collaboration. DESI 2024 VI: Cosmological Constraints from the Measurements of Baryon Acoustic Oscillations. *arXiv* **2024**, arXiv:2404.03002.
39. DES Collaboration. Dark Energy Survey: A 2.1% measurement of the angular Baryonic Acoustic Oscillation scale at redshift $z_{eff} = 0.85$ from the final dataset. *arXiv* **2024**, arXiv:2402.10696.
40. Scolnic, D.M.; Jones, D.O.; Rest, A.; Pan, Y.C.; Chornock, R.; Foley, R.J.; Huber, M.E.; Kessler, R.; Narayan, G.; Riess, A.G.; et al. The Complete Light-curve Sample of Spectroscopically Confirmed SNe Ia from Pan-STARRS1 and Cosmological Constraints from the Combined Pantheon Sample. *Astron. J.* **2018**, *859*, 101. [CrossRef]
41. Jimenez, R.; Loeb, A. Constraining Cosmological Parameters Based on Relative Galaxy Ages. *Astrophys. J.* **2002**, *573*, 37. [CrossRef]
42. Handley, W.J.; Hobson, M.P.; Lasenby, A.N. POLYCHORD: Nested sampling for cosmology. *Mon. Not. R. Astron. Soc. Lett.* **2015**, *450*, L61–L65. [CrossRef]
43. Lewis, A. GetDist: A Python package for analysing Monte Carlo samples. Instrumentation and Methods for Astrophysics. *arXiv* **2019**, arXiv:1910.13970.
44. Lozano Torres, J.A. Testing Cosmic Acceleration from the Late-Time Universe. *Astronomy* **2023**, *2*, 300–314. [CrossRef]
45. Kazantzidis, L.; Perivolaropoulos, L. Evolution of the $f\sigma 8$ tension with the Planck15/ΛCDM determination and implications for modified gravity theories. *Phys. Rev. D* **2018**, *97*, 103503. [CrossRef]
46. Akaike, H. A new look at the statistical model identification. *IEEE Trans. Autom. Control.* **1974**, *19*, 716–723. [CrossRef]
47. Schwarz, G. Estimating the Dimension of a Model. *Ann. Statist.* **1978**, *6*, 461–464. [CrossRef]
48. Cong, Z.; Han, Z.; Shuo, Y.; Siqi, L.; Tong-Jie, Z.; Yan-Chun, S. Four new observational H(z) data from luminous red galaxies in the Sloan Digital Sky Survey data release seven. *Res. Astron. Astrophys.* **2014**, *14*, 1221
49. Simon, J.; Verde, L.; Jimenez, R. Constraints on the redshift dependence of the dark energy potential. *Phys. Rev. D* **2005**, *71*, 123001. [CrossRef]
50. Moresco, M.; Cimatti, A.; Jimenez, R.; Pozzetti, L.; Zamorani, G.; Bolzonella, M.; Dunlop, J.; Lamareille, F.; Mignoli, M.; Pearce, H.; et al. Improved constraints on the expansion rate of the Universe up to z $\approx$ 1.1 from the spectroscopic evolution of cosmic chronometers. *J. Cosmol. Astropart. Phys.* **2012**, *8*, 6. [CrossRef]
51. Moresco, M.; Pozzetti, L.; Cimatti, A.; Jimenez, R.; Maraston, C.; Verde, L.; Thomas, D.; Citro, A.; Tojeiro, R.; Wilkinson, D. A 6 percent measurement of the Hubble parameter at z $\approx$ 0.45: Direct evidence of the epoch of cosmic re-acceleration. *J. Cosmol. Astropart. Phys.* **2016**, *5*, 14. [CrossRef]
52. Ratsimbazafy, A.L.; Loubser, S.I.; Crawford, S.M.; Cress, C.M.; Bassett, B.A.; Nichol, R.C.; Väisänen, P. Age-dating luminous red galaxies observed with the Southern African Large Telescope. *Mon. Not. R. Astron. Soc.* **2017**, *467*, 3239–3254. [CrossRef]
53. Stern, D.; Jimenez, R.; Verde, L.; Kamionkowski, M.; Stanford, S.A. Cosmic chronometers: Constraining the equation of state of dark energy. I: H(z) measurements. *J. Cosmol. Astropart. Phys.* **2010**, *2*, 8. [CrossRef]
54. Borghi, N.; Moresco, M.; Cimatti, A. Toward a Better Understanding of Cosmic Chronometers: A New Measurement of H(z) at z $\approx$ 0.7. *Astrophys. J. Lett.* **2022**, *928*, L4. [CrossRef]
55. Jiao, K.; Borghi, N.; Moresco, M.; Zhang, T.-J. New Observational H(z) Data from Full-spectrum Fitting of Cosmic Chronometers in the LEGA-C Survey. *Astrophys. J. Suppl. Ser.* **2023**, *265*, 48. [CrossRef]
56. Tomasetti, E.; Borghi, N.; Moresco, M.; Jiao, K.; Cimmatti, A.; Pozzetti, L.; Carnall, A.C.; McLure, R.J.; Pentericci, L. A new measurement of the expansion history of the Universe at z = 1.26 with cosmic chronometers in VANDELS. *Astron. Astrophys.* **2023**, *265*, 48. [CrossRef]
57. Moresco, M. Raising the bar: New constraints on the Hubble parameter with cosmic chronometers at z $\approx$ 2. *Astrophys. J. Suppl. Ser.* **2023**, *A96*, 18. [CrossRef]
58. Nunes, R.C.; Yadav, S.K.; Jesus, J.F.; Bernui, A. Cosmological parameter analyses using transversal BAO data. *Mon. Not. R. Astron. Soc.* **2020**, *497*, 2133–2141. [CrossRef]
59. Nunes, R.C.; Bernui, A. BAO signatures in the 2-point angular correlations and the Hubble tension. *Eur. Phys. J. C.* **2020**, *80*, 1025. [CrossRef]
60. Verde, L.; Bernal, J.L.; Heavens, A.F.; Jimenez, R. The length of the low-redshift standard ruler. *Mon. Not. R. Astron. Soc.* **2017**, *467*, 731–736. [CrossRef]
61. Lemos, T.; Ruchika; Carvalho, J.C.; Alcaniz, J. Low-redshift estimates of the absolute scale of baryon acoustic oscillations. *Eur. Phys. J. C* **2023**, *83*, 495. [CrossRef]
62. Pogosian, L.; Zhao, G.-B.; Jedamzik, K. Recombination-independent Determination of the Sound Horizon and the Hubble Constant from BAO. *Astrophys. J. Lett.* **2020**, *904*, L7. [CrossRef]
63. Luongo, O.; Muccino, M. Model independent cosmographic constraints from DESI 2024. *arXiv* **2024**, arXiv:2404.07070.

64. Carloni, Y.; Luongo, O.; Muccino, M. Does dark energy really revive using DESI 2024 data. *arXiv* **2024**, arXiv:2404.12068.
65. Liu, G.; Wang, Y.; Zhao, W. Impact of LRG1 and LRG2 in DESI 2024 BAO data on dark energy evolution. *arXiv* **2024**, arXiv:2407.04385.
66. Giare, W.; Najafi, M.; Pan, S.; Di Valentino, E.; Firouzjaee, J.T. Robust Preference for Dynamical Dark Energy in DESI BAO and SN Measurements. *arXiv* **2024**, arXiv:2407.16689.
67. Dinda, B.R.; Maartens, R. Model-agnostic assessment of dakr energy after DESI DR1 BAO. *arXiv* **2024**, arXiv:2407.17252.
68. Jiang, J.-Q.; Giare, W.; Gariazzo, S.; Dainotti, M.G.; Di Valentino, E.; Mena, O.; Pedrotti, D.; Santos da Costa, S.; Vagnozzi, S. Neutrino cosmology after DESI: Tightest mass upper limits, preference for the normal ordering, and tension with terrestrial observations. *arXiv* **2024**, arXiv:2407.18047.